Intrinsic Electronic Transitions of the Absorption Spectrum of $(OPy)_2Ti(TAP)_2$: Implications Toward Photostructural Modifications

Channa R. De Silva,[†,§] J. David Musgraves,[†] Z. Schneider,[||] B. G. Potter, Jr.,[†] T. J. Boyle,[⊥] K. Simmons-Potter,[‡,||] and L. René Corrales*[,†,§]

Department of Materials Science and Engineering, Department of Electrical and Computer Engineering, Department of Chemistry, and College of Optical Science, The University of Arizona, Tucson, Arizona 85721, and Sandia National Laboratories, Albuquerque, New Mexico 87106

Received: February 20, 2009

Theoretical calculations based on time-dependent density functional theory are used to characterize the electronic absorption spectrum of a heteroleptic Ti-alkoxide molecule, $(OPy)_2Ti(TAP)_2$ [OPy = pyridine carbinoxide, TAP = 2,4,6 tris(dimethylamino)phenoxide] under investigation as a photosensitive precursor for use in optically initiated solution synthesis of the metal oxide. Computational results support the assignment of UV absorption features observed in solid-state precursor films to key intrinsic ground-state transitions that involve ligand-to-metal charge transfer and $\pi-\pi^*$ transitions within the cyclic ligand moieties present. The nature of electron density redistribution associated with these transitions provides early insight into the excitation wavelength dependence of photostructural modification previously observed in this precursor system.

Direct photoexcitation of intermolecular linking reactions in metal alkoxide systems during the initial stages of material formation provides a new opportunity to manipulate the evolution of metal oxide network topology and, therefore, the ensuing nano- to microstructure detail in solution-derived materials. Experimental investigations of engineered, water-stable heteroleptic transition metal alkoxides have demonstrated the opportunity to selectively disrupt ligand moieties leading to hydrolysis and condensation via UV exposure.[1−7] The process has also been used to enable the photoinduced, patterned deposition of partially condensed oxide material directly from solution.[8−10] Our recent studies show that the photoexposure of $(OPy)_2Ti(TAP)_2$ in both solid-state and water/pyridine solution initiates the hydrolysis and condensation reactions that lead to sol−gel type Ti−O−Ti bridging molecular assemblies.[11] While optical spectroscopic analysis of the resulting photoproducts provides insight into the effects of optical excitation, missing is detailed insight into the specific excitation and reaction pathways responsible for these effects. Of particular interest is the observed excitation wavelength dependency of the photostructural effects where the photoexposure of $(OPy)_2Ti(TAP)_2$ at $\lambda = 248$ nm leads to significant modifications of the structure, forming condensation products, whereas limited photostructural modifications are observed at $\lambda = 337$ nm excitation.[11] This suggests that the effectiveness of photoinduced ligand destabilization (leading to hydrolysis and condensation) is linked to the nature of the specific electronic transitions accessed upon optical excitation. A characterization of excited-state molecular electronic configurations for states participating in ground-state optical absorption processes would thus provide important insight into charge redistribution accompanying optical excitation and its potential impact on the propensity for ligand reactivity.

In this work, time-dependent density functional theory (TDDFT) was used to characterize the excited-state energetics and associated electronic density redistribution in $(OPy)_2Ti(TAP)_2$. These results are compared to the ground-state electronic absorption spectrum of a solid-state thin film of the same alkoxide precursor. The ramifications of these results on potential optical excitation paths for photostructural change are discussed.

The synthesis and characterization of $(OPy)_2Ti(TAP)_2$ have been previously reported.[12] A stock solution of $(OPy)_2Ti(TAP)_2$ was generated by dissolving 0.048 g of the precursor material into 2 mL of anhydrous pyridine, producing a 30 mM concentration, under glovebox conditions. This solution was stirred for 30 min prior to use to ensure proper mixing. Following mixing of the solution, thin films of the material were obtained by spin coating; 0.35 mL of solution was deposited onto a 1×1 in.^{2} fused silica substrate and spun at 350 rpm for 30 s. Spun films were retained in the glovebox for 4 days to allow for the evaporation of any residual pyridine from the film.

Absorption spectra were collected in the wavelength range between 200 and 800 nm, with a wavelength resolution of 1 nm, using a Perkin-Elmer Lambda 950 UV/vis spectrometer. Additionally, ellipsometry measurements were taken in the same area as the absorption spectrum to determine film thickness ($d = 76$ nm) and index of refraction ($n_{632.8\ nm} = 1.585$).

All calculations were performed at the level of density functional theory (DFT) using the NWChem package developed at the Environmental Molecular Sciences Laboratory, Pacific Northwest National Laboratory (PNNL).[13] The hybrid B3LYP exchange correlation functional was employed.[14−16] Geometry optimization of the $(OPy)_2Ti(TAP)_2$ complex was carried out without symmetry constraints. The energy-consistent relativistic effective core potentials (RECPs) developed by the Stuttgart group (Stuttgart RSC 1997 ECP)[17] were used for the Ti(IV) center with the optimized valence basis sets supplemented by polarization functions. Standard 6-311+G* Gaussian basis

* To whom correspondence should be addressed. E-mail: lrcorral@email.arizona.edu.
† Department of Materials Science and Engineering.
‡ Department of Electrical and Computer Engineering.
§ Department of Chemistry.
|| College of Optical Science.
⊥ Sandia National Laboratories.

10.1021/jp9016008 CCC: $40.75
Published on Web 04/16/2009

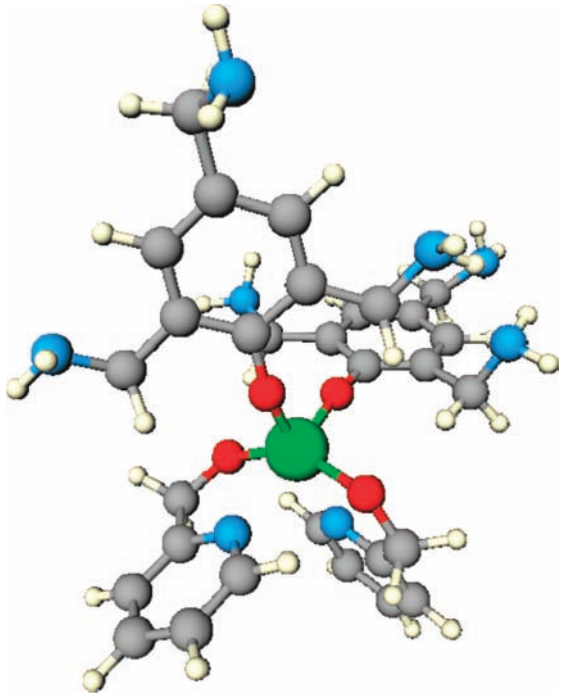

Figure 1. Optimized molecular structure of $Ti(TAP)_2(Opy)_2$. Color scheme: red (O); blue (N); gray (C); white (H); green (Ti).

TABLE 1: Calculated Bond Distances and Angles of $(OPy)_2Ti(TAP)_2$

bond distances (Å)		bond angles (°)	
Ti−O(OPy-1)	1.901	O(TAP-1)−Ti−N(Opy-2)	169.9
Ti−O(OPy-2)	1.902	N(Opy-1)−Ti−O(TAP-2)	167.4
Ti−N(OPy-1)	2.307	O(OPy-1)−Ti−O(OPy-2)	148.0
Ti−N(OPy-2)	2.338		
Ti−O (TAP-1)	1.823		
Ti−O (TAP-2)	1.830		

functions were employed for the C, H, N, and O atoms. The vertical excitation energies and the oscillator strengths at the optimized ground-state geometries were obtained by TDDFT calculations implemented in NWChem 5.0.[18]

The optimized calculated molecular structure of the title complex is shown in Figure 1, and the calculated bond distances and angles (of the first coordination sphere) are summarized in Table 1. The coordination sphere is very similar to the recently reported family of mononuclear $Ti(O)_2(OPy)_2$ complexes forming a distorted octahedron.[12] These calculations show that the N atom of the Lewis basic pyridine moiety of each OPy ligand binds to the Ti(IV) metal in addition to the O atom of the alcohol of each OPy. The chelating binding determined by our calculations is consistent with the experimental X-ray crystal structures of other related families of compounds. (It is important to note that this material is available only as an oil, and, hence, its true crystal structure remains unavailable.)

The calculated average Ti−O(OPy) (1.90 Å) and Ti−N(OPy) (2.32 Å) bond distances are in agreement with the literature X-ray crystallographic results: 1.89 and 2.23 Å in $(OPy)_2Ti(DMP)_2$ (DMP = 2,6-dimethylphenol), 1.89 and 2.24 Å in $(OPy)_2Ti(DIP)_2$ (DIP = 2,6-diisopropylphenol), and 1.89 and 2.22 Å in $(OPy)_2Ti(DPP)_2$ (DPP = 2,6-diphenylphenol), respectively.[12] The calculated average Ti−O (TAP) bond distance (1.83 Å) is also within agreement of the literature Ti−O distances in phenyl-substituted DMP (1.87 Å), DIP (1.86 Å), or DPP (1.87 Å) ligands.[12]

Gaussian peaks corresponding to the UV−vis absorption spectrum were generated by successive fitting routines using

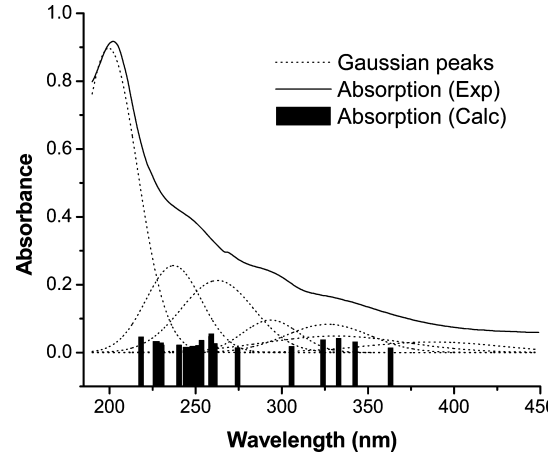

Figure 2. UV−vis absorption characteristics of $(OPy)_2Ti(TAP)_2$.

TABLE 2: Comparison of Gaussian Peak Maxima and Calculated Energies

Gaussian peak λ_{max} (nm)	calculated excitation energy (nm)	oscillator strength
237	229	0.02887
	230	0.0225
	240	0.02255
263	259	0.05576
	261	0.02702
294	305	0.01854
327	333	0.04266

the Peakfit program (version 4.05 SPSS Inc.) ($r^2 = 0.99$) to identify the major electronic transition regions in the spectrum. Calculated Gaussian line shapes and TDDFT-B3LYP vertical excitation energies are shown in Figure 2. The Gaussian peaks overlap well with the calculated electronic transitions at 237, 263, 294, and 327 nm (Table 2). Note that a group of electronic transitions centered around 248 nm are found to lie within the overlapping area of the second and third Gaussian peaks.

A molecular orbital analysis shows that the highest occupied molecular orbital (HOMO) and HOMO−1 (the second to the highest occupied MO) of $(OPy)_2Ti(TAP)_2$ originate primarily from the TAP ligands. In contrast, the lowest unoccupied molecular orbital (LUMO) is localized on both Ti(IV) metal and OPy ligands (Figures 3 and S1). Detailed MO analysis shows that electronic transitions in the range of 274−400 nm (Gaussian peak regions centered at 327 and 294 nm) are primarily based on ligand-to-metal charge transfer (LMCT) transitions. This analysis is done by assigning the calculated excited states (given in units of nanometer) to their coorresponding electronic transitions as determined from MO analysis, for example: 363 (HOMO to LUMO+5), 342 (HOMO−1 to LUMO+5), 333 (HOMO to LUMO+7), 323 (HOMO−1 to LUMO+4), and 305 (HOMO−1 to LUMO+7), and 274 (HOMO to LUMO+9). Here LUMO+4 and LUMO+5 orbitals are based purely on Ti(IV) d orbitals. From theses electron density maps, given in terms of MOs, it is straightfortward to determine that the electron density oringinally located on the TAP moiety in the ground states moves to the Ti(IV) metal center and the opposing OPy ligand groups in the excited state. This type of transition is then indentified with LMCT states observed in these systems. The MO analysis of the electronic excited states in the range of 259−218 nm reveal that those transitions are primarily based on ligand π-to-π^* transitions with some charge transfer character (see Figure 3 and the Supporting Information). The calculated electronic transitions at 259, 258,

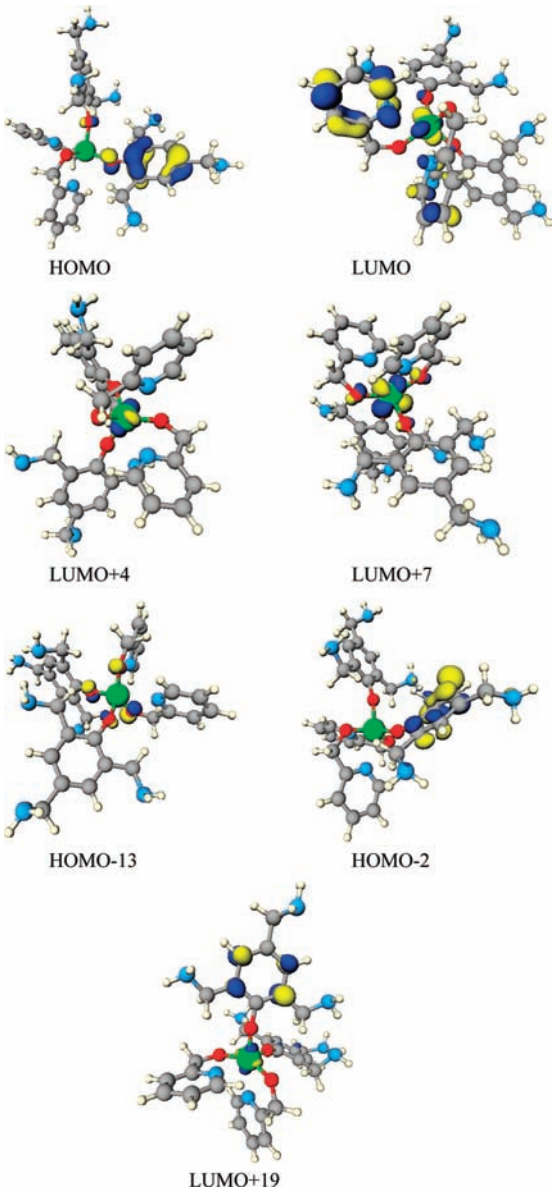

Figure 3. Representative 3D isosurfaces of the Kohn−Sham molecular orbitals involved in electronic transitions; see text.

251, and 247 nm were determined to originate from electrons in the p orbitals of coordinated oxygen atoms. The electronic transitions at 259 and 247 nm are based on the electronic transitions from HOMO−13 to LUMO and HOMO−11 to LUMO+5, respectively. Note that HOMO−13 and HOMO−11 molecular orbitals are based on oxygen p orbitals of both OPy and TAP ligands (Figures 3 and S2).

The direct excitation of the ligands leading to the transitions associated with the oxygen-coordinated orbitals in this particular region of the absorption spectrum appears consistent with enhanced efficiency of ligand disruption leading to hydrolysis and condensation observed experimentally via vibrational spectroscopy after the photoexposure of the complex at 248 nm.[11] An excitation channel involving coordinated oxygen-based molecular orbitals may initiate the dissociation of Ti−O bonds leading toward the formation of photodissociated products at the excitation wavelength of 248 nm. However, involvement of such oxygen-based molecular orbitals is minimum or negligible in the LMCT transitions observed above 274 nm of the UV−vis spectrum. This observation is consistent with the negligible photoinduced structural response of $(OPy)_2Ti(TAP)_2$ observed after irradiation at 337 nm.[11]

In addition to the electronic transitions originating from oxygen-based p-type orbitals, our calculations show that π-to-π^* transitions involving TAP ligand aromatic rings were also evident in the high energy UV region. For example, the absorption features at 230 and 226 nm are due to the electronic transitions from HOMO−1 to LUMO+16 and HOMO−2 to LUMO+19 orbitals, respectively (Figure 3 and the Supporting Information). These orbitals are localized mainly on TAP ligands confirming the TAP ligand-based π-to-π^* transitions. This latter finding also supports the general tendency for preferential disruption of the TAP-ligand moiety upon 248 nm irradiation as observed in prior vibrational studies of precursor photoresponse.[8,11]

In summary, the electronic transitions observed in the UV−vis spectrum of $(OPy)_2Ti(TAP)_2$ were identified and the nature of the excited states were evaluated using TDDFT calculations. LMCT transitions were identified as the excitation mechanism for excitation wavelengths longer than 274 nm in agreement with similar transistions observed in related complexes. Transitions in the range of 259−218 nm are primarily based on π-to-π^* with some minor charge transfer character and are further associated with the TAP moiety present in the precursor molecule. The π-to-π^* electronic transitions originating from coordinated oxygen-based molecular orbitals are likely responsible for the enhanced photosensitivity observed experimentally for precursor systems irradiated in this wavelength regime, leading to the formation of photoproducts consistent with hydrolysis and condensation.[11] In contrast, excitation in the longer wavelength range is resonant with ligand-to-metal charge transfer processes, suggesting a difference in the associated response of the molecule. This supports the reduced photoactivity previously observed at 337.1 nm in solution and solid-state precursor specimens.[8,11]

These computations represent the first analysis of the nature of the excited states in this complex, photoactive metal-alkoxide structures, and, moreover, provide increased insight into the photoexcitation mechanisms leading to photocatalysis of key network-forming reactions in the context of photodirected, solution-phase synthesis of oxide materials.

Acknowledgment. This work was supported by (CRDS, LRC) start-up funds from the University of Arizona. Acknowledgement is also made to the Donors of The Petroleum Research Fund, administered by the American Chemical Society. The calculations were performed in part using the Molecular Science Computing Facility in the Environmental Molecular Sciences Laboratory, a national scientific user facility sponsored by the U.S. Department of Energy's Office of Biological and Environmental Research and located at PNNL. Images were produced using the Extensible Computational Chemistry Environment (ECCE).

Supporting Information Available: Figure S1, 3D isosurfaces of the Kohn−Sham molecular orbitals involved in LMCT transitions. Figure S2, 3D isosurfaces of the Kohn−Sham molecular orbitals involved in originating π-to-π^* electronic transitions. Table S1, calculated TDDFT-B3LYP electronic transitions and their oscillator strengths in the range of 259−218 nm. This material is available free of charge via the Internet at http://pubs.acs.org.

References and Notes

(1) Segawa, H.; Adachi, Y. A.; Yoshida, K. *J. Am. Ceram. Soc.* **2003**, *86*, 761.

(2) Kim, H. R.; Park, O. H.; Choi, Y. K.; Bae, B. S. *J. Sol. Gel. Sci. Technol.* **2000**, *19*, 607.
(3) Watanabe, A.; Miyashita, T. *Chem. Lett.* **2006**, *35*, 1130.
(4) Soppera, O.; Moreira, P. J.; Leite, A. P.; Marques, P. V. S. *J. Sol.-Gel. Sci. Technol.* **2005**, *35*, 27.
(5) Tohge, N.; Ueno, R.; Chiba, F.; Kintaka, K.; Nishi, J. *J. Sol.-Gel. Sci. Technol.* **2000**, *19*, 119.
(6) Segawa, H.; Tateishi, K.; Arai, Y.; Yoshida, K.; Kaji, H. *Thin Solid Films* **2004**, *466*, 48.
(7) Ohya, T.; Nakayama, A.; Ban, T.; Ohya, Y.; Takahashi, Y. *Bull. Chem. Soc. Jpn.* **2003**, *76*, 429.
(8) Musgraves, J. D.; Potter, B. G. J.; Boyle, T. J. *Opt. Lett.* **2008**, *33*, 1306.
(9) Musgraves, J. D.; Potter, B. G. J.; Sewell, R. M.; Boyle, T. J. *J. Mater. Res.* **2007**, *22*, 1694.
(10) Kololuoma, T.; Karkkainen, A. H. O.; Tolonen, A.; Rantala, J. T. *Thin Solid Films* **2003**, *440*, 184.
(11) Potter, B. G. J.; Musgraves, J. D.; Boyle, T. J. *J. Non-Cryst. Solids* **2008**, *354*, 2017.
(12) Boyle, T. J.; Sewell, R. M.; Ottley, L. A. M.; Pratt, H. D.; Quintana, C. J.; Bunge, S. D. *Inorg. Chem.* **2007**, *46*, 1825.
(13) Bylaska, E. J.; de Jong, W. A.; Kowalski, K.; Straatsma, T. P.; Valiev, M.; Wang, D.; Apra, E.; Windus, T. L.; Hirata, S.; Hackler, M. T.; Zhao, Y.; Fan, P. D.; Harrison, R. J.; Dupuis, M.; Smith, D. M. A.; Nieplocha, J.; Tipparaju, V.; Krishnan, M.; Auer, A. A.; Nooijen, M.; Brown, E.; Cisneros, G.; Fann, G. I.; Fruchtl, H.; Garza, J.; Hirao, K.; Kendall, R.; Nichols, J. A.; Tsemekhman, K.; Wolinski, K.; Anchell, J.; Bernholdt, D.; Borowski, P.; Clark, T.; Clerc, D.; Dachsel, H.; Deegan, M.; Dyall, K.; Elwood, D.; Glendening, E.; Gutowski, M.; Hess, A.; Jaffe, J.; Johnson, B.; Ju, J.; Kobayashi, R.; Kutteh, R.; Lin, Z.; Littlefield, R.; Long, X.; Meng, B.; Nakajima, T.; Niu, S.; Pollack, L.; Rosing, M.; Sandrone, G.; Stave, M.; Taylor, H.; Thomas, G.; van Lenthe, J.; Wong, A.; Zhang, Z. *NWChem, A Computational Chemistry Package for Parallel Computers*, 5.0; Pacific Northwest National Laboratory: Richland, WA, 2006.
(14) Becke, A. D. *J. Chem. Phys.* **1993**, *98*, 5648.
(15) Lee, C.; Yang, W.; Parr, R. G. *Phys. Rev. B* **1988**, *37*, 785.
(16) Becke, A. D. *Phys. Rev. A* **1988**, *38*, 3098.
(17) Dolg, M., *Effective Core Potentials in Modern Methods and Algorithms of Quantum Chemistry*; John von Neumann Institute for Computing: Julich, 2000; Vol. 1, p 479.
(18) Hirata, S.; Head-Gordon, M. *Chem. Phys. Lett.* **1999**, *314*, 291.

JP9016008